THE FASEB JOURNAL • RESEARCH • www.fasebj.org

Hypoxic niches are endowed with a protumorigenic mechanism that supersedes the protective function of PTEN

Carlos H. V. Nascimento-Filho,[*,†] Liana P. Webber,[*,‡] Gabriell B. Borgato,[*,§] Eny M. Goloni-Bertollo,[†] Cristiane H. Squarize,[*,¶,1] and Rogerio M. Castilho[*,¶,1,2]

[*]Laboratory of Epithelial Biology, Department of Periodontics and Oral Medicine, School of Dentistry, University of Michigan, Ann Arbor, Michigan, USA; [†]Genetics and Molecular Biology Research Unit, Department of Molecular Biology, School of Medicine of São José do Rio Preto, São Paulo, Brazil; [‡]Department of Oral Pathology, School of Dentistry, Federal University of Rio Grande do Sul, Porto Alegre, Rio Grande do Sul, Brazil; [§]Department of Oral Biology, School of Dentistry, State University of Campinas, Piracicaba, São Paulo, Brazil; and [¶]University of Michigan Comprehensive Cancer Center, Ann Arbor, Michigan, USA

ABSTRACT: Head and neck squamous cell carcinoma (HNSCC) is the sixth most common malignancy worldwide and is characterized by a fast-paced growth. Like other solid tumors, the HNSCC growth rate results in the development of hypoxic regions identified by the expression of hypoxia-inducible factor 1α (HIF-1α). Interestingly, clinical data have shown that pharmacological induction of intratumoral hypoxia caused an unexpected rise in tumor metastasis and the accumulation of cancer stem cells (CSCs). However, little is known on the molecular circuitries involved in the presence of intratumoral hypoxia and the augmented population of CSCs. Here we explore the impact of hypoxia on the behavior of HNSCC and define that the controlling function of phosphatase and tensin homolog (PTEN) over HIF-1α expression and CSC accumulation are de-regulated during hypoxic events. Our findings indicate that hypoxic niches are poised to accumulate CSCs in a molecular process driven by the loss of PTEN activity. Furthermore, our data suggest that targeted therapies aiming at the PTEN/PI3K signaling may constitute an effective strategy to counteract the development of intratumoral hypoxia and the accumulation of CSCs.—Nascimento-Filho, C. H. V., Webber, L. P., Borgato, G. B., Goloni-Bertollo, E. M., Squarize, C. H., Castilho, R. M. Hypoxic niches are endowed with a protumorigenic mechanism that supersedes the protective function of PTEN. FASEB J. 33, 13435–13449 (2019). www.fasebj.org

KEY WORDS: ROS · mTOR · EMT · epithelial-mesenchymal transition · cancer stem cell

Head and neck cancer is one of the 10 most common cancers in the United States (1). In recent years, there were significant advances in the understanding of the genetic landscape of head and neck squamous cell carcinoma (HNSCC) and the molecular signaling network commonly found disrupted in human papillomavirus and non–human papillomavirus oral and pharyngeal cancers. Yet, the 5-yr relative survival rate of patients afflicted with this disease have marginally improved in the last decades.

Much of the complexity in managing oral and pharyngeal cancer relies on the heterogeneity of cancer cells, the numerous mutations found in HNSCC, and the presence of cancer cells presenting self-renewability. The cellular heterogeneity adds to the complexity of the tumors and the low success rates of monotherapies when compared with multidrug regiments. Antiangiogenic agents like sunitinib and bevacizumab are currently in use for several solid tumors. However, the long-term benefits are restricted to a moderate increase in progression-free survival, and little benefit is observed when considering the overall survival of patients treated for HNSCC (2). The administration of antiangiogenic drugs leads to metastasis and tumor relapse short after treatment (3, 4). Not only antiangiogenic drugs increase the chance for metastasis

ABBREVIATIONS: ALDH, aldehyde dehydrogenase; ALDH1, aldehyde dehydrogenase 1; ALDH1A1, aldehyde dehydrogenase 1 family, member A1; BpV(pic), bisperoxovanadium inhibitor of protein phosphotyrosine phosphatase; BrdU, bromodeoxyuridine/5-bromo-2′-deoxyuridine; CSC, cancer stem cell; EMT, epithelial-mesenchymal transition; FBS, fetal bovine serum; GAPDH, glyceraldehyde 3-phosphate dehydrogenase; H&E, hematoxylin and eosin; HIF-1α, hypoxia-inducible factor 1α; HNSCC, head and neck squamous cell carcinoma; mTOR, mammalian target of rapamycin; NANOG, nanog homeobox; NDRG2, N-Myc downstream-regulated gene 2; pS6, phosphorylated S6; PTEN, phosphatase and tensin homolog; ROS, reactive oxygen species; shRNA, short hairpin RNA; siRNA, small interfering RNA; SNAI1, snail family transcriptional repressor 1; VIM, vimentin

[1] These authors contributed equally to this work.

[2] Correspondence: Laboratory of Epithelial Biology, Department of Periodontics and Oral Medicine, University of Michigan, 1011 N University Ave., Room 2029c, Ann Arbor, MI 48109-1078, USA. E-mail: rcastilh@umich.edu

doi: 10.1096/fj.201900722R

This article includes supplemental data. Please visit *http://www.fasebj.org* to obtain this information.

but also modifies the tumor microenvironment by creating intratumoral hypoxia (5). Early studies also demonstrated that hypoxic conditions prime the activation of the PI3K-signaling pathway in prostate cancer and human embryonic kidney cell lines (6, 7). Interestingly, we have previously shown that phosphatase and tensin homolog (PTEN), a master regulator of mammalian target of rapamycin (mTOR) signaling, directly controls the population of epithelial stem cells (8) and the PI3K/mTOR pathway (9–11), suggesting that this pathway may also play a role in regulating cancer stem cells (CSCs). Here we aim to identify the effects of hypoxia over the tumor suppressor gene PTEN and the impact over HNSCC behavior.

Our findings showed that hypoxic conditions primed PTEN de-regulation in HNSCC along with the induction of an epithelial-mesenchymal transition (EMT) phenotype and enhanced invasive properties. The hypoxic niches detected in HNSCC xenografts lack PTEN activity and increases the number of cancer cells positive for aldehyde dehydrogenase 1 family, member A1 (ALDH1A1). We also found that pharmacological inhibition of PTEN recapitulated the effects of hypoxia by triggering the expression of hypoxia-inducible factor 1α (HIF-1α) and the accumulation of CSCs followed by the acquisition of an EMT invasive phenotype.

MATERIALS AND METHODS

Cell lines, PTEN inhibitor, and oxygen absorbers

HNSCC cell lines WSU-HN6 (base of tongue), WSU-HN12 (lymph node/metastasis), and WSU-HN13 (tongue) were cultured in DMEM (HyClone Laboratories, Logan, UT, USA) supplemented with 10% fetal bovine serum (FBS; Thermo Fisher Scientific, Waltham, MA, USA) and 1% antibiotic-antimycotic (Thermo Fisher Scientific). Cells were maintained in a 5% CO_2-humidified incubator at 37°C (*https://seer.cancer.gov/statfacts/html/oralcav.html*). All cells were previously authenticated by PCR amplification of short tandem repeats to ensure cell identity. Cells were maintained under hypoxia for 6, 12, and 24 h as previously reported (12–15). Hypoxic conditions were achieved by placing tumor cell lines in a plastic slider bag along with 2000 cc oxygen absorber pouches containing active powdered iron oxide (BayTec Containers, Bacliff, TX, USA). The oxygen absorption was monitored using an oxygen meter (Pro Gas Badge; Grainger, Lake Forest, IL, USA). Cells were considered under hypoxic conditions upon oxygen levels drop under 2%. All cells exposed to hypoxia were maintained in a 5% CO_2-humidified incubator at 37°C. The PTEN inhibitor bisperoxovanadium inhibitor of protein phosphotyrosine phosphatase [BpV(pic)] was administered for 24 h at the final concentrations of 1, 5, and 10 μM. Time course assay was performed using 5 μM of BpV(pic) at the time points of 24, 30, 36, and 48 h. For each time point, cells were fixed and processed for immunofluorescence and photos were taken using a Axiocan ERc5s color camera (Zeiss, Munich, Germany) attached to a Nikon Eclipse Ts2 (Nikon, Tokyo, Japan) and visualized with Nikon Elements NIS software.

Xenografts and tumor volume measurements

In vivo study was performed according to the University of Michigan Institutional Animal Care & Use Committee approved protocol and in compliance with the *Guide for the Care and Use of Laboratory Animals* [National Institutes of Health (NIH), Bethesda, MD, USA]. Female nude mice Foxn1(nu) (The Jackson Laboratory, Bar Harbor, ME, USA) 4–6-wk-old mice were housed in 12-h light/dark cycles, and they received standard rodent chow and water *ad libitum* in compliance with Association for Assessment and Accreditation of Laboratory Animal Care guidelines. A total of 5×10^6 WSU-HN12 cells were bilaterally injected into mice's flanks + 50% DMEN + 50% Matrigel (Corning, Corning, NY, USA). Tumor length and width were measured 3 times weekly using a digital caliper, and tumor volume were calculated using the formula $V = (W^2 \times L)/2$ as previously described (16, 17). Body weight was also assessed 3 times weekly. All procedures were in agreement with the approved animal handling protocol. At the end point of each group, mice were euthanized and tumors were collected. Tumors reaching the maximum size allowed by University Committee for the Use and Care of Animals were also euthanized. Estimated daily tumor growth was calculated according to previous studies (16, 18, 19). All tumors were formalin fixed and paraffin embedded.

Short hairpin RNA, small interference RNA knockdown, plasmids, and lentivirus

Lentiviral vectors pGIPZ expressing control short hairpin RNA (shRNA) or *PTEN*-shRNA (Dharmacon, Lafayette, CO, USA).

Lentiviral vectors were packaged in HEK 293T cells transfected with psPAX2 and pMD2G plasmids (Trono Lab; Addgene, Watertown, MA, USA). At 72 h post-transfection, medium containing lentivirus was collected and filtered through a 0.4-μM filter, and WSU-HN13 cells were transduced in the presence of 4 μg/ml polybrene (MilliporeSigma, Burlington, MA, USA). Cell populations stably expressing shRNAs were selected in medium containing 1 μg/ml puromycin (MilliporeSigma). Knockdown efficiencies of shRNAs against *PTEN* in these cells were determined by Western blot analysis. HIF-1α knockdown was achieved using small interfering RNA (siRNA) technology as previously described by Zagni *et al.* (8). Cells were seeded in 24-well plates and transfected with siRNA duplex against human HIF-1α (forward 5′-CUGAUGACCAGCAACUUGA-3′ and reverse 5′-UCAAGUUGCUGGUCAUCAG-3′) (20). The optimal concentration was determined by dilution curves of siRNA and immunoblot analyses. The sequences of the control negative siRNA oligonucleotides were as follows: 5′-UUCUCCGAACGUGUCACGUTT-3′ and 5′-ACGUGACACGUUCGGAGAATT-3′.

Invasion assay

HNSCC tumor cells (WSU-HN6, WSU-HN12, and WSU-HN13) were seeded in 24-well plates over a thin homogeneous layer of fibronectin (BD Biosciences, San Jose, CA, USA) in Millicell Cell Culture Inserts (MilliporeSigma) and supplemented with 2% of FBS in the upper side and 10% of FBS lower side. Tumor cells from the control group were maintained under normal O_2 levels and the hypoxia group under $<2\%$ O_2. After 24 h of cellular invasion, cells were stained with hematoxylin and eosin (H&E), and the total number of cells located at the upper chamber and the lower chamber (invasive cells) were quantified. Images of the selected fields were captured using a color camera (Micropublisher 5.0; QImaging, Surrey, BC, Canada) at a magnification of ×40 attached to a Nikon Eclipse 80i microscope (Nikon). The images were analyzed using the ImageJ program (NIH).

Immunofluorescence and histologic studies

Tissues derived from xenograft tumor were fixed using 4% paraformaldehyde for 24 h and further embedded in paraffin and

sectioned (4 μm of thickness). Histologic sections were deparaffinized in xylene solution and rehydrated in a descending ethanol series. Antigen retrieval was performed using citric acid followed by blocking for unspecific binding using 0.5% (v/v) Triton X-100 in PBS and 3% (w/v) bovine serum albumin. Tissue sections were incubated overnight with primary antibodies anti–HIF-1α, anti-PTEN (Cell Signaling Technology, Danvers, MA, USA) and anti-ALDH1A (Abcam, Cambridge, MA, USA). Tissue samples were then washed with 1× PBS and incubated with Alexa Fluor 488 or 568 secondary antibodies (Thermo Fisher Scientific) for 60 min at room temperature and then stained with DNA staining Hoechst 33342 (Thermo Fisher Scientific) for visualization of DNA content. Images were taken using a QImaging ExiAqua monochrome digital camera attached to a Nikon Eclipse 80i microscope and H&E stained slides were photographed using a color camera (QImagingMicropublisher 5.0) attached to a Nikon Eclipse 80i microscope (Nikon) and processed using Nikon Elements NIS software.

Flow cytometry

HNSCC CSCs were identified by its high content levels of aldehyde dehydrogenase 1 (ALDH1) enzymatic activity and positivity to CD44 expression using flow cytometry (BD Biosciences, San Jose, CA, USA). The Aldefluor Kit (Stemcell Technologies, Durham, NC, USA) was used according to the manufacturer's instructions to identify cells with high ALDH1 enzymatic activity. Briefly, ALDH1 is a detoxifying enzyme responsible for the oxidation of intracellular aldehydes as previously published by Charafe-Jauffret *et al.* (21). Normal and cancer cells expressing high levels of ALDH1 have been shown to contain stem/progenitor properties compared with cells expressing low levels of the enzyme (22–26). Aldefluor is a nonimmunologic method that exposed the endogenous cellular levels of ALDH1 to the fluorescent substrate that diffuses into the cells that are catalyzed by the aldehyde dehydrogenase (ALDH) enzyme releasing a negative charged ALDH product that can be detected by flow cytometry using a 488 nM laser. We combined the use of ALDH with the expression levels of CD44 to identify HNSCC CSCs, as previously reported by Prince *et al.* (27). Cells under hypoxic conditions or receiving BpV(pic) were suspended with activated Aldefluor substrate [boron-dipyrromethene (BODIPY) amino acetate] or negative control (dimethylamino benzaldehyde, a specific ALDH inhibitor) for 45 min at 37°C. Then, cells were washed and suspended with anti-CD44/allophycocyanin conjugated antibody and incubated for 25 min in shaking rotor at 4°C. All samples were analyzed using a flow cytometer Accuri C6 (BD Biosciences) equipped with 2 excitation lasers: a solid blue state (488 nm) and a diode red (640 nm).

Reactive oxygen species/superoxide detection kit

We measured reactive oxygen or superoxide species production in live cells using a flow cytometer Accuri C6 (BD Biosciences). The oxidative stress detection reagent (Green) and superoxide detection reagent (Orange) were reconstituted following the manufacturer's recommendations (Enzo Life Sciences, East Farmingdale, NY, USA). Reactive oxygen species (ROS) detection dye (green probe) reacts with multiples reactive species as hydrogen peroxide, peroxynitrite, hydroxyl radical, NO, and peroxy radical. Meanwhile, the superoxide detection dye (orange probe) reacts with superoxide (O_2^-).

Bromodeoxyuridine/5-bromo-2′-deoxyuridine staining protocol

Cellular DNA synthesis was performed using the FITC Bromodeoxyuridine/5-bromo-2′-deoxyuridine (BrdU) Flow Kit (BD Biosciences) and flow cytometric analysis. The process of incorporation of BrdU into newly synthesized DNA initiates with the administration of BrdU (15 μg/μl) for 15 min, followed by fixation and permeabilization of tumor cells using BD Cytofix, followed by the permeabilization using Cytoperm buffers for 15–30 min at room temperature. After washing, cells were incubated with DNase in Dulbecco's phosphate-buffered saline (DPBS) for 1 h at 37°C at a final concentration of 300 μg/ml. Cells were resuspended in 50 μl of BD Perm/Wash Buffer containing diluted FITC fluorochrome-conjugated anti-BrdU antibody and 7-amino-actinomycin D to detect total DNA content and incubated for 20 min at room temperature. After washing, cells were analyzed by flow cytometry.

Western blot

Tumor cells were lysed with cell lysis buffer containing protease inhibitors and briefly sonicated. Total protein was run in SDS-PAGE and transferred to an Immobilon Membrane (MilliporeSigma). PVDF membranes were blocked in 5% nonfat dry milk containing 0.1 M Tris (pH 7.5), 0.9% NaCl, and 0.05% Tween-20 for 1 h at room temperature followed by the incubation with anti-PTEN (Cell Signaling Technology) 1:1000, anti–N-Myc downstream-regulated gene 2 (NDRG2) (Cell Signaling Technology) 1:1000, or antivimentin (VIM) (AMF-17b; Developmental Studies Hybridoma Bank, Iowa City, IA) 1:1000 and anti–glyceraldehyde 3-phosphate dehydrogenase (GAPDH) mouse mAb (6C5) (MilliporeSigma) primary antibodies overnight at 4°C. PVDF membranes were then incubated with appropriate secondary antibodies conjugated to horseradish peroxidase (Santa Cruz Biotechnology, Dallas, TX, USA). The signal was developed using the ECL Western Blotting Substrate (Pierce Biotechnology, Rockford, IL, USA).

RNA extraction and RT-PCR

HNSCC cells were harvested using trypsin [0.05% trypsin-EDTA (1x)], and the RNA was extracted with E.Z.N.A. Total Kit I (Omega Bio-Tek, Norcross, GA, USA) following the manufacturer's protocol. RNA concentration and purity were determined by spectrophotometer (NanoDrop 1000 Spectrophotometer; Thermo Fisher Scientific), measuring absorbance at A_{260} and A_{280} nm. A total of 100 μg RNA was reverse transcribed with a High Capacity cDNA Reverse Transcription Kit (Thermo Fisher Scientific) according to the manufacturer's instructions. For real-time quantitative PCR analyses, the reaction mixture containing cDNA template, primers, and SYBR Green PCR Master Mix (Thermo Fisher Scientific) were run in a 7900 HT Real-time PCR System (Thermo Fisher Scientific). Fold changes of mRNA levels were determined after normalization to reference control of GAPDH β-actin levels. The $2^{-\Delta\Delta Ct}$ method of relative quantification were used to estimate the copy number of gene expression. Primer sequences for *GAPDH*, *β-ACTIN*, nanog homeobox (*NANOG*), and *TWIST1* primers were designed using the PrimerBank database, and primer sequences for snail family transcriptional repressor 1 (*SNAI1*) and *VIM* were previously published by Flores *et al.* (28).

GAPDH: 5′-ACCCACTCCTCCACCTTTGAC-3′; 5′-CCACCACCCTGTTGCTGTAG-3′
β-ACTIN: 5′-AAATCTGGCACCACACCTTC-3′; 5′-GGGGTGTTGAAGGTCTCAAA-3′
SNAI1: 5′-GCGTGTGCTCGGACCTTCT-3′; 5′-ATCCTGAGCAGCCGGACTCT-3′
TWIST: 5′-AAGCTGAGCAAGATTCAGACC-3′; 5′-CGTGAGCCACATAGCTGC-3′
VIM: 5′-GACGCCATCAACACCGAGTT-3′; 5′-CTTTGTCGTTGGTTAGCTGGT-3′

NANOG: 5′-CCCCAGCCTTTACTCTTCCTA-3′; 5′-CCAGGTTGAATTGTTCCAGGTC-3′

Statistical analysis

Statistical analysis was performed using Prism 7 (GraphPad Software, La Jolla, CA, USA). Statistical tests used were 1-way ANOVA and Student's *t* tests. Data are expressed as means ± SEM. Significance was determined when $P \leq 0.05$, $P \leq 0.01$, $P \leq 0.001$, or $P \leq 0.0001$. No significance was determined when $P > 0.05$.

RESULTS

HNSCC under hypoxic conditions undergoes EMT and increases the invasive behavior

Solid tumors, including HNSCCs, are characterized by fast-growing and local invasion capabilities. During rapid cell division and increased tumor mass, solid tumors often undergo hypoxia. The effects of hypoxia on solid tumors are of interest to cancer biologists because recent findings suggest increased aggressive behavior and the development of a resistant phenotype to chemo and radiotherapies. Here we investigated the potential implications of hypoxic conditions in the behavior of HNSCC. We observed that low oxygen levels (~2% of O_2) induced the expression of HIF-1α in cancer cells along with an epithelial transition to a spindle shape (**Fig. 1*A, B***). Indeed, all tumor cells undergoing morphologic changes were associated with the accumulation of cytoplasmic VIM, a stromal cellular biomarker that identifies epithelial cells undergoing EMT (Fig. 1*C*). Notably, all analyzed tumor cell lines growing under hypoxic conditions were characterized by an enhanced cellular invasion phenotype (1.38–2.56-fold increase) (Fig. 1*D*). Indeed, when analyzing all 3 HNSCC cell lines, we found that nearly 75% of all seeded WSU-HN6 cells have invaded the substrate compared with 30% of tumor cells invading in normoxia (Fig. 1*E*). WSU-HN12 also presented an increased percentage of invading cells from 10 to ~20%, whereas WSU-HN13 demonstrated an increase in tumor invasion from 40 to ~60% of all seeded cells (Fig. 1*E*). Although exciting, we observed that some tumor cell lines cultured under hypoxia had a high mortality rate when compared with normoxia. With this in mind, we evaluated the effect of hypoxia on cellular viability. The WSU-HN12 and WSU-HN13 had a significant reduction in the total number of cells when cultured under hypoxic conditions (Fig. 1*F*). Reduced viability of tumor cells upon hypoxia did not reflect in a reduced number of invasive cells as we have shown previously in Fig. 1*D, E*, suggesting that hypoxia was selecting and inducing surviving cells to display aggressive behavior. Indeed, the WSU-HN6 cell line, which expressed the highest number of invading cells (2.56-fold increase), responded to hypoxia by increasing cell viability above normoxia levels (Fig. 1*F*). Overall, we observed that despite reduced cellular viability mediated by harsh hypoxic conditions, the HNSCC tumor cells enhanced their aggressive invasive phenotype when exposed to hypoxia (Fig. 1*G*).

Hypoxia ablates the tumor suppressor PTEN and triggers HIF-1α activation

The administration of antiangiogenic drugs has been associated with the development of intratumoral hypoxia and enhanced metastatic potential. The tumor suppressor gene *PTEN* is found down-regulated in cancer, yet the presence of mutations constitutes a rare event in HNSCC. Moreover, the mechanisms involved in the deregulation of *PTEN* in solid tumors, including HNSCC, are largely unknown. Here we evaluated the levels of PTEN on HNSCC under hypoxia. We found that PTEN is deactivated by hypoxia (**Fig. 2*A–F***). Notably, the PTEN deactivation occurred in a time-dependent manner (Fig. 2*A–C*). We also observed a reduction on *PTEN* mRNA levels within 24 h of exposure to hypoxic conditions (Supplemental Fig. S1*A*). Hypoxia-induced PTEN ablation also led to the activation of the PI3K/mTOR signaling demonstrated by the presence of the biomarker phosphorylated S6 (pS6) (Fig. 2*D–F*). Notably, the absence of PTEN due to hypoxia was also observed in the hypoxic niches *in vivo*. Similar to primary human HNSCC tumors presenting fast growth rate and displaying the formation of multiple tumor islands composed of concentric squamous malignant epithelial cells (**Fig. 3*A***), our HNSCC xenograft models ($n = 5$) also developed typical histologic characteristics of fast-growing tumors (Fig. 3*B*).

Furthermore, our xenograft animals are characterized by the presence of hypoxic niches, which were determined by the high levels of HIF-1α (Fig. 3*C*). Similar to our *in vitro* observations (Fig. 2*A–C*), intratumoral hypoxic niches failed to express PTEN (Fig. 3*D*). This observation is more evident in the Fig. 3*E, F* in which PTEN is observed in green-labeled malignant cells (Fig. 3*F*, arrows) next to the hypoxic niche (Fig. 3*F*, red). Interesting to note that surrounding the hypoxic niches, we observe the expression of PTEN in fusiform shaped cells, suggestive of mesenchymal origin (Supplemental Fig. S1*B*, arrowheads). To better understand the correlation between tumor suppressor PTEN and the hypoxic niches, we asked whether PTEN would participate in hypoxic signaling by modulating HIF-1α. Using shRNA technology, we found that down-regulation of PTEN (Fig. 3*G*) trigger the accumulation of the protein levels of HIF-1α (Fig. 3*H, I*). Further, we explored if HIF-1α is involved in the induction of EMT, or if the observed phenotype is driven by PTEN down-regulation during hypoxia. Using siRNA technology, we have observed that depletion of HIF-1α does not result in the accumulation of VIM in HNSCC cultured under hypoxia when compared with controls that presented modest accumulation of VIM during hypoxia (Supplemental Fig. S2*A, B*). Depletion of HIF-1α from tumor cells undergoing hypoxia also failed to trigger the accumulation of fusiform tumor cells above baseline levels observed during hypoxic conditions, or during the pharmacological inhibition of PTEN [BpV(pic)] (Supplemental Fig. S2*C, D*).

Altogether, these novel findings demonstrated that the expression of HIF-1α is controlled by PTEN in HNSCC and that hypoxic niches are involved in the deregulation of the tumor suppressor PTEN (Fig. 3*J*).

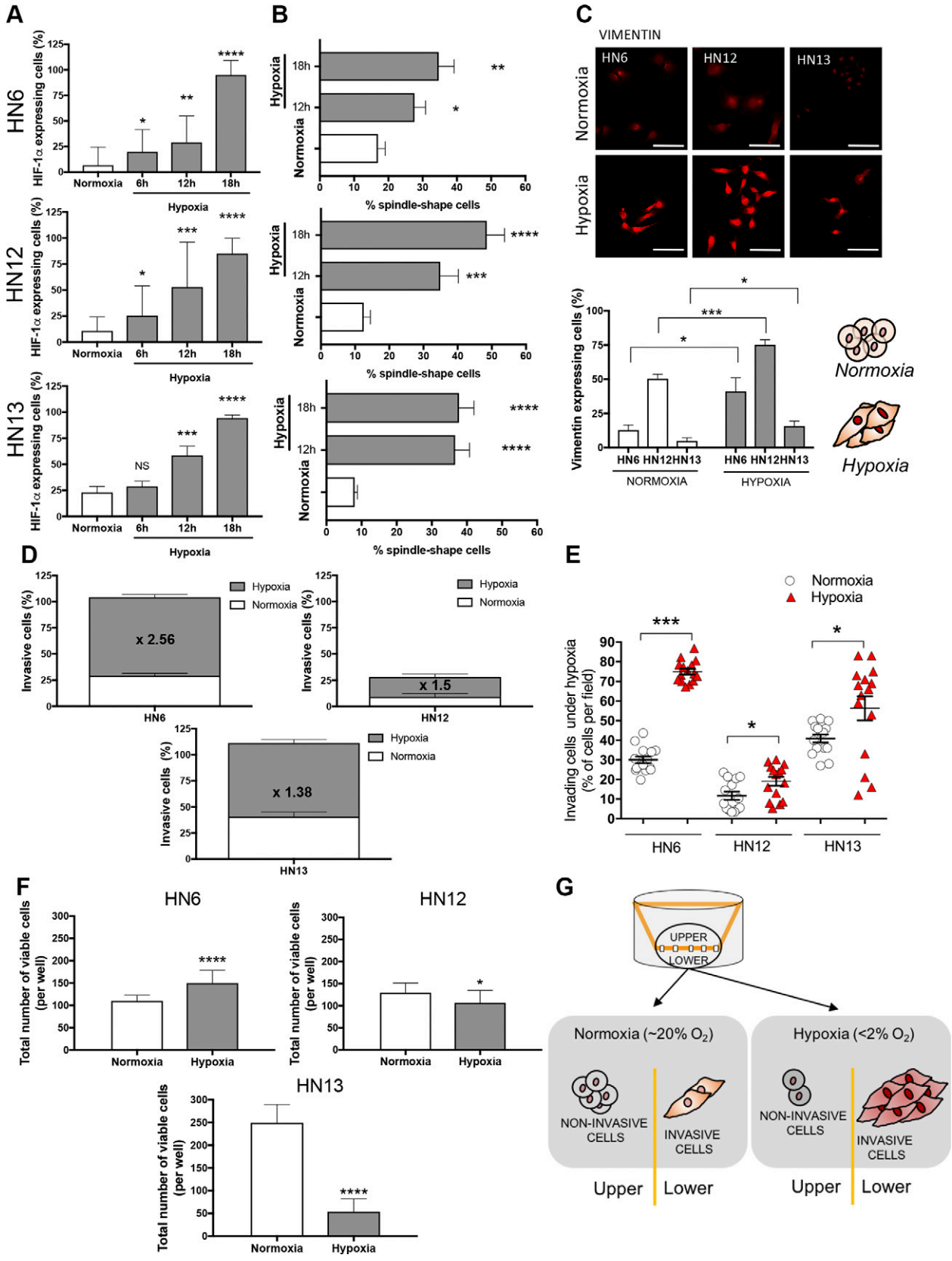

Figure 1. HNSCC cell under hypoxic conditions underwent EMT phenotype and enhanced invasive behavior. *A*) Time course assay of 3 HNSCC cell lines growing under hypoxic conditions depict increased expression of HIF-1α compared with normoxic controls. Data represent means ± SEM. $*P < 0.05$, $**P < 0.01$, $***P < 0.001$, $****P < 0.0001$. *B*) HNSCC cell lines under hypoxic conditions presenting spindle-shaped phenotype compared with normoxic condition. Data represent means ± SEM. $*P < 0.05$, $**P < 0.01$, $***P < 0.001$, $****P < 0.0001$. *C*) Immunofluorescence for VIM of HNSCC cells cultured under hypoxia (24 h).

(*continued on next page*)

PTEN down-regulation triggers EMT and stemness-associated markers

Our previous data show that HNSCC exposed to hypoxic conditions underwent EMT and reduced the levels of PTEN. Here we explored the correlation between PTEN deregulation and the activation of EMT phenotype using the chemical compound BpV(pic), a known PTEN inhibitor (**Fig. 4*A***). We found that the BpV(pic) mechanism of action involves the down-regulation of NDRG2, a PTEN-binding protein responsible for the recruitment of PP2A and consequently dephosphorylation of PTEN (active form) (Fig. 4*A*) (29). Reduced levels of NDRG2 leads to the activation of the PI3K/AKT signaling pathway and its downstream target (30). We also found that HNSCC receiving BpV(pic) acquires a fusiform phenotype similar to the one observed during hypoxic conditions (Fig. 4*B*). Indeed, the EMT could be observed after 30 h of BpV(pic) administration with a peak on the morphology alterations occurring after 48 h (Fig. 4*B*). Furthermore, administration of BpV(pic) also triggered HIF-1α up-regulation along with the activation of the PI3K/mTOR signaling pathway (Fig. 4*C–E*) like previously observed during hypoxic conditions (Figs. 1 and 2). To further test our hypothesis that PTEN loss of function induces EMT and potentially modulates CSCs, we evaluated the expression changes of key genes associated with EMT and stemness by real-time PCR. We found that VIM, Nanog, and Snail were found up-regulated upon exposure to hypoxic conditions and BpV(pic) (Fig. 4*F, G*). Similarly, tumor cells cultured under hypoxic conditions also demonstrate the genetic EMT signature with up-regulation of VIM, Snail, and Nanog along with Twist-1 (Fig. 4*G*). Down-regulation of PTEN during hypoxia was confirmed by the reduced expression levels of *NDRG2* (Fig. 4*H*). All things considered, we observed that deregulation of PTEN driven by hypoxia or BpV(pic) not only activates HIF-1α but concomitantly activates mTOR signaling along with the induction of EMT (Fig. 4*I*).

Deregulation of PTEN impact the accumulation of ROS and dampers apoptosis from tumor cells

Many factors are orchestrated to induce cellular apoptosis. Much of these factors are associated with the expression of tumor suppressor genes like *TP53* and *PTEN*. The accumulation of ROS and superoxide are critical events in the activation of programmed cell death (31, 32). Here we found that BpV(pic)-induced deregulation of PTEN also down-regulates the levels of ROS and superoxide in HNSCC cells (**Fig. 5*A***). Aligned with the low levels of ROS and superoxide, we observed that HNSCC cells became resistant to apoptosis (Fig. 5*B, C*) and undergoing G2/M suggestive of cellular proliferation (Fig. 5*D*). Interestingly, however, a fraction of tumor cells expressing low levels of PTEN undergo a transitory G0/G1 cell cycle arrest, an event suggestive of cellular quiescence (33, 34) (Fig. 5*E*). Although exciting, the fact that BpV(pic)-treated tumor cells can display 2 distinct behaviors, cellular proliferation, and cellular quiescence intrigued us. To better understand these results, we reassessed the flow cytometry data in the search for distinct populations of tumor cells capable of responding differently to PTEN inhibition. Indeed, we found that both populations, 1 undergoing G_2/M cell cycle phase, and the other undergoing G_0/G_1 cell cycle are distinct by cell size and internal complexity as judged by the side scatter and forward scatter profile (Fig. 5*F*). Altogether, our data suggest that reduced levels of the tumor suppressor gene *PTEN* lead to an apoptosis-resistant phenotype and the accumulation of 2 distinct populations of tumor cells, 1 highly mitogenic, and the second population in a quiescent-like stage (Fig. 5*G*).

Hypoxia-induced down-regulation of PTEN results in the accumulation of CSCs

Our previous data indicate that PTEN inhibition triggers a transitory G0/G1 cell cycle arrest, a strong indication of cellular quiescence (Fig. 5*E*). This finding prompted us to explore if hypoxic conditions could favor the accumulation of HNSCC CSCs, as recently suggested in breast cancer (5). Poised by this fascinating hypothesis, we decided to explore the presence of CSCs during hypoxic conditions using flow cytometry to identify the enzymatic activity of ALDHs (**Fig. 6*A***). Interestingly, we found that hypoxic HNSCC tumor cells present a significant accumulation of CSCs when compared with normoxic conditions (Fig. 6*B, C*). To further confirm if the effects of hypoxia over the PTEN signaling was indeed deemed responsible for the accumulation of CSCs, we decided to pharmacologically inhibit PTEN using BpV(pic). We found that BpV(pic)-driven reduced levels of PTEN lead to the accumulation of CSCs as judged by the combined increased levels of ALDH enzymatic activity detected by Aldefluor, and high levels of CD44 positive cells (Fig. 6*D, E*). Mechanistically, we know that hypoxia induces the down-regulation of PTEN that

Lower graphics depict the percentage of cancer cells expressing VIM under normoxia and hypoxia culture conditions. Data represent means ± SEM. Scale bars, 100 μm. $*P < 0.05$, $***P < 0.001$. *D*) Increased folds of tumor invasion of WSU-HN6 (2.56), WSU-HN12 (1.5), and WSU-HN13 (1.38) cell lines upon invasion assay under hypoxic conditions. *E*) Augmented invasion of hypoxic WSU-HN6, WSU-HN12, and WSU-HN13 cell lines compared with tumor cells invading in normoxia. Data represent means ± SEM. $*P < 0.05$, $***P < 0.001$. *F*) Quantification of the total number of viable tumor cells after 24 h of invasion at the upper and lower chambers (initial seeding density of 10^4 cells). Note the higher number of WSU-HN6 tumor cells under hypoxia compared with the lower number of WSU-HN12 and WSU-HN13 cells compared with normoxic conditions. Data represent means ± SEM. $*P < 0.05$, $****P < 0.0001$. *G*) Schematic representation of the enhanced invasion of tumor cells during hypoxia.

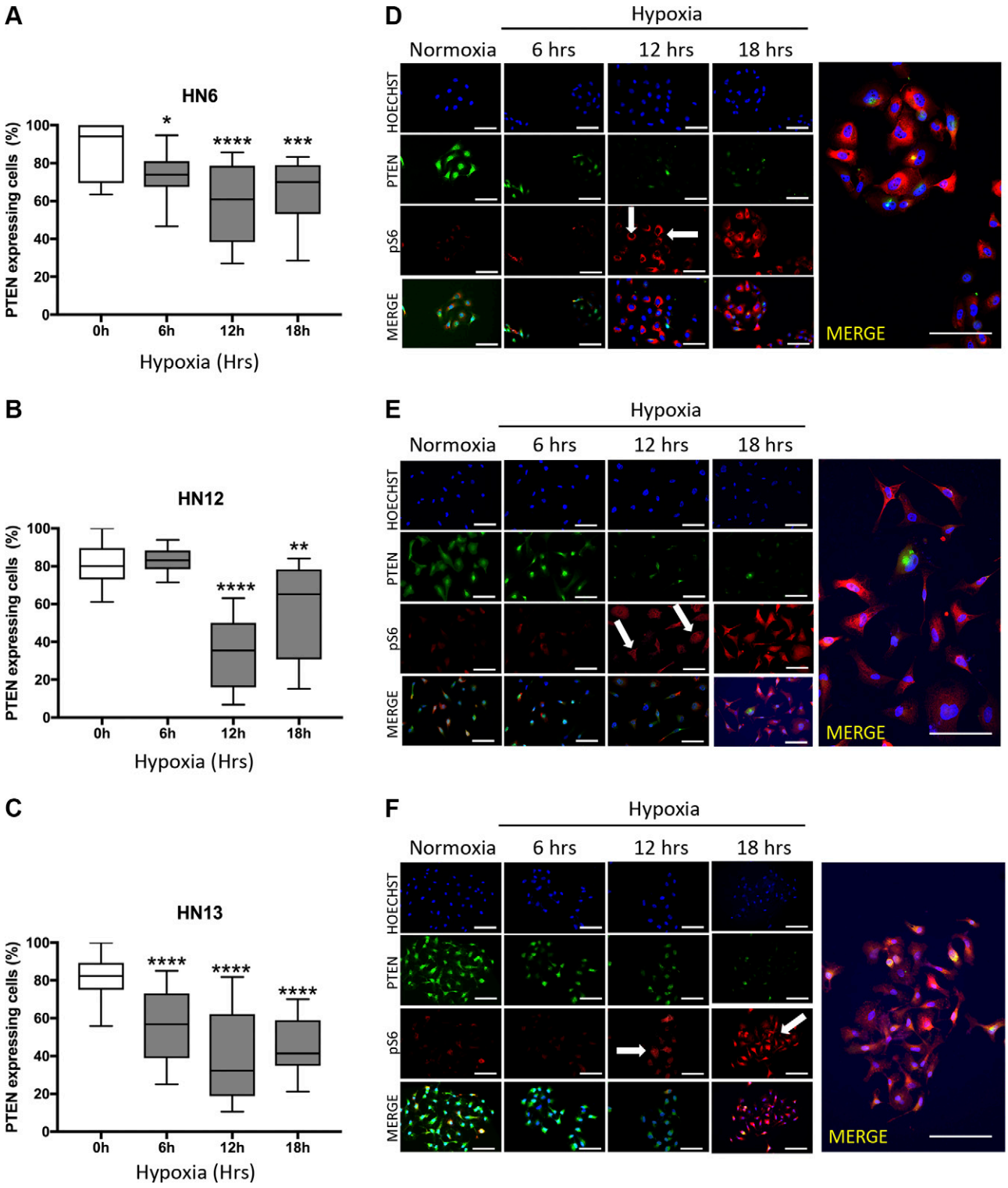

Figure 2. PTEN down-regulation during hypoxia. *A–C*) Time course assay for PTEN expression levels in head and neck cancer cell lines cultured under hypoxic conditions and compared with normoxic controls Data represent means ± SEM. $*P < 0.05$, $**P < 0.01$, $***P < 0.001$, $****P < 0.0001$. Note that all analyzed cancer cell lines present reduced levels of PTEN when cultured under hypoxia. *D–F*) Representative images from WSU-HN6, WSU-HN12, and WSU-HN13 cell lines cultured under the hypoxic condition for up to 18 h. Immunofluorescence staining for PTEN depicts down-regulation of the tumor suppressor starting after 6 h of hypoxia for WSU-HN6 and WSU-HN13 and after 12 h for WSU-HN12 compared with normoxic controls. pS6 staining was used as a readout for the activation of the PTEN/PI3K-signaling pathway. Arrows indicate high expression of pS6 after 12 h of hypoxia in all tested HNSCC cell lines. Scale bars, 100 μm.

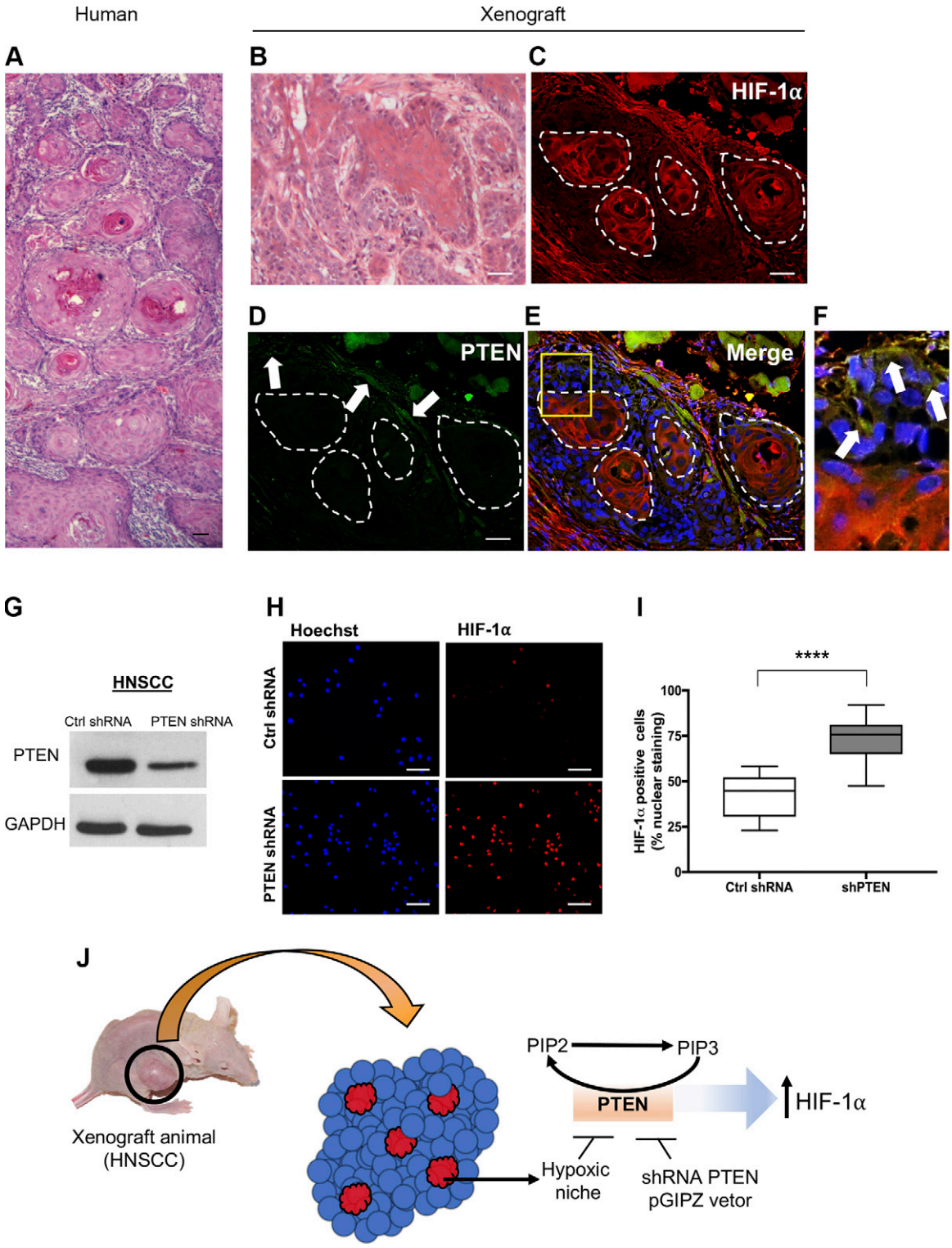

Figure 3. Genetic deregulation of PTEN induces HIF-1α expression. *A*) Tumor sample (H&E) from a human HNSCC depicts the formation of a typical morphologic aspect of a fast-growing HNSCC displaying the development of multiple tumor islands composed of concentric squamous malignant epithelial cells. *B*) Normal histologic architecture of xenograft-derived squamous cell carcinoma (H&E) presenting tumor islands depicting different degrees of cellular differentiation. *C–F*) Immunofluorescence staining of squamous cell carcinoma xenografts displaying HIF-1α staining conjugated with Alexa 568 (*C*), PTEN staining conjugated with Alexa 488 (*D*, arrows), merge of all 3 channels (*E*) presenting cells positive for PTEN within the tumor mass (*F*, arrows), and within the hypoxic niche, and hypoxic areas (red). *G*) Down-regulation of protein levels of PTEN upon delivery of PTEN-shRNA. *H*) Representative image of HNSCC cells expressing high levels of HIF-1α detected by immunofluorescence after delivery of PTEN-shRNA. *I*) Quantification of the total number of HIF-1α–positive cells from tumor cells receiving PTEN-shRNA compared with control shRNA (scrambled shRNA). ****$P < 0.0001$. *J*) Schematic representation of hypoxic niches and the expression of PTEN-driven expression of HIF-1α. Scale bars, 100 μm.

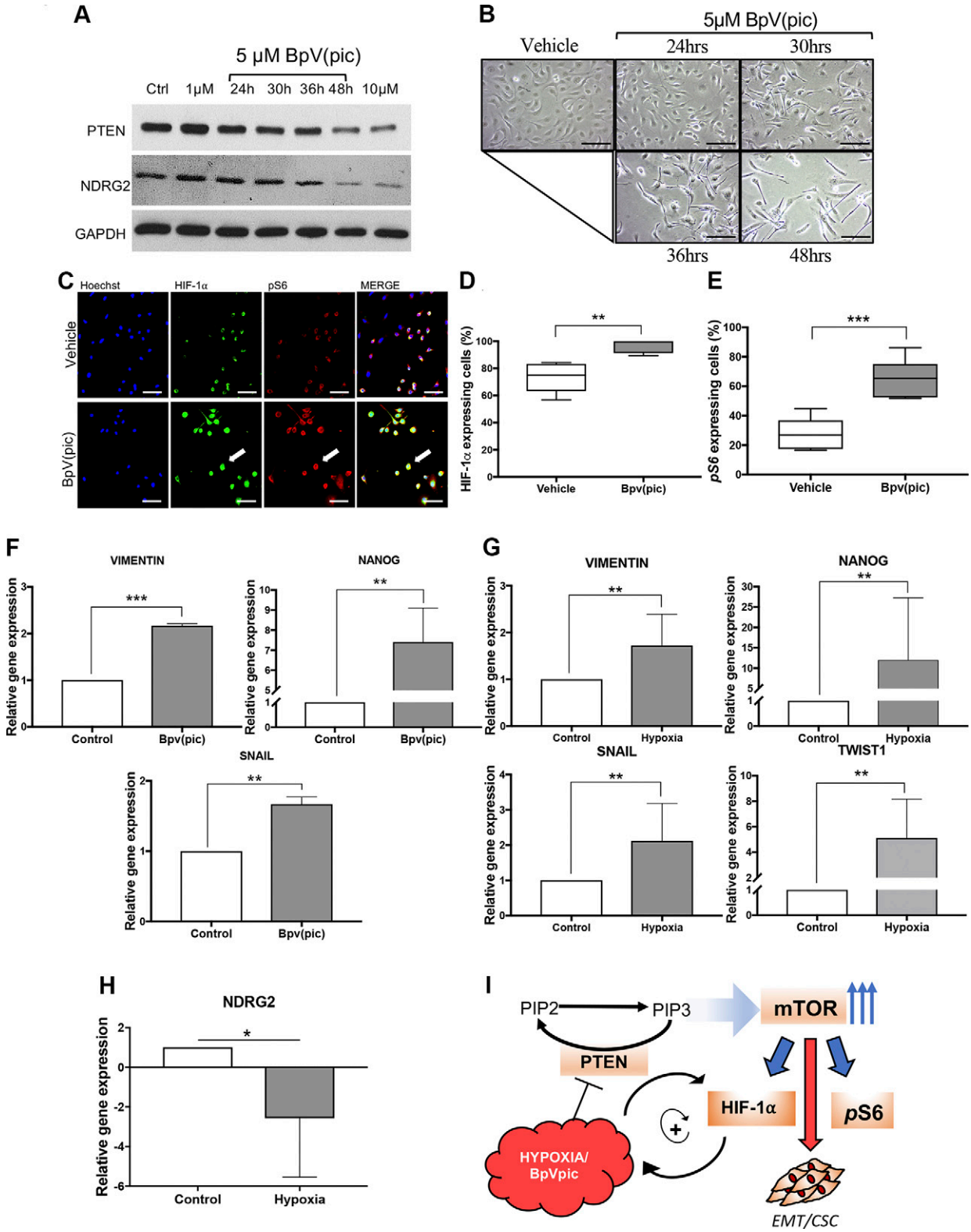

Figure 4. Pharmacological down-regulation of PTEN activates HIF-1α expression and triggers an EMT phenotype on HNSCC. *A*) Administration of BpV(pic) efficiently down-regulated PTEN and NDRG2 after 48hrs of treatment. *B*) HNSCC tumor cells exposed to BpV(pic) acquire a fusiform phenotype. *C*) Administration of BpV(pic) triggers the accumulation of HIF-1α and pS6 as demonstrated by immunofluorescence staining. Note colocalization of HIF-1α and pS6 in tumor cells (arrow). *D, E*) Quantification of HIF-1α (*D*) and pS6 (*E*) immunostainings upon administration of BpV(pic). $^{**}P < 0.01$, $^{***}P < 0.001$. *F*) Real-time PCR of HNSCC cells receiving the PTEN inhibitor BpV(pic) demonstrate up-regulation of VIM, Snail, and Nanog genes. $^{***}P < 0.001$, $^{****}P < 0.0001$. *G*) Tumor cells growing under hypoxic conditions also present higher gene expression levels of VIM, Snail, and Nanog, along with Twist-1. $^{*}P < 0.05$, $^{***}P < 0.001$, $^{****}P < 0.0001$. *H*) Real-time PCR demonstrate down-regulation of NDRG2 in head and neck cell line during hypoxic conditions. $^{***}P < 0.001$. *I*) Schematic representation of similar effects of hypoxia and BpV(pic) on the down-regulation of PTEN, followed by the up-regulation of HIF-1α and pS6. Scale bars, 100 μm.

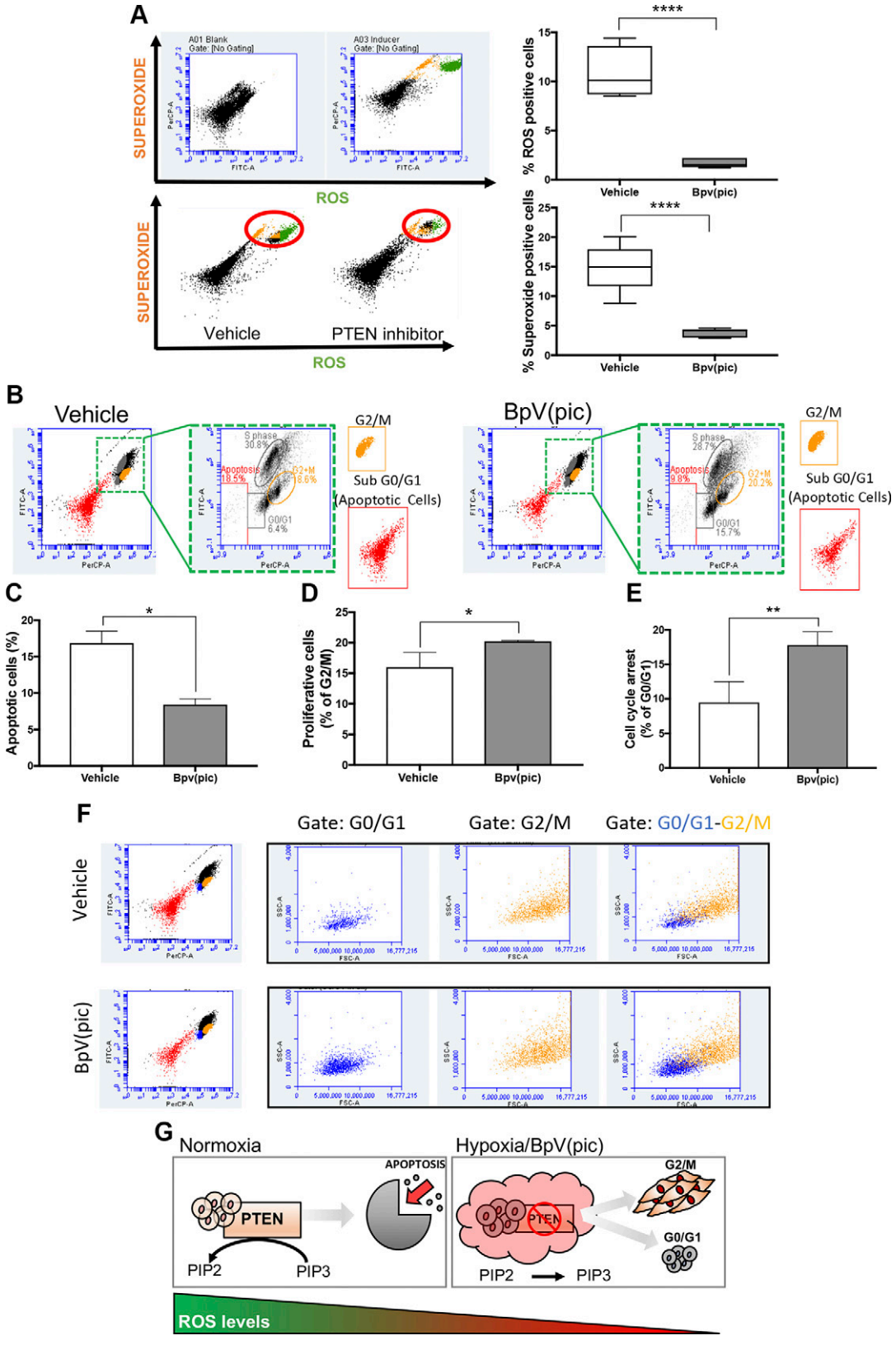

Figure 5. PTEN inhibition reduces ROS and enhances tumor proliferation. *A*) Flow cytometry for ROS and superoxide of HNSCC cells receiving 5 μM BpV(pic) or vehicle for 48 h. Note reduced levels of ROS and superoxide upon administration of BpV(pic). Data represent means ± SEM. $^{****}P < 0.0001$. *B–D*) Detection of DNA synthesis using BrdU combined with flow cytometry demonstrate reduced apoptosis and increased proliferation of tumor cells receiving BpV(pic). Data represent means ± SEM. $^{*}P < 0.05$. *E*) Detection of DNA synthesis using BrdU combined with flow cytometry also identified a population of tumor cells undergoing G_0/G_1 upon administration of BpV(pic). *F*) Flow cytometry analysis identifies 2 distinct populations of tumor cells under G_0/G_1 and G_2/M. *G*) Schematic representation of PTEN inhibition associated with reduced ROS levels and reduced apoptosis, resulting in augmented tumor proliferation of HNSCC cells.

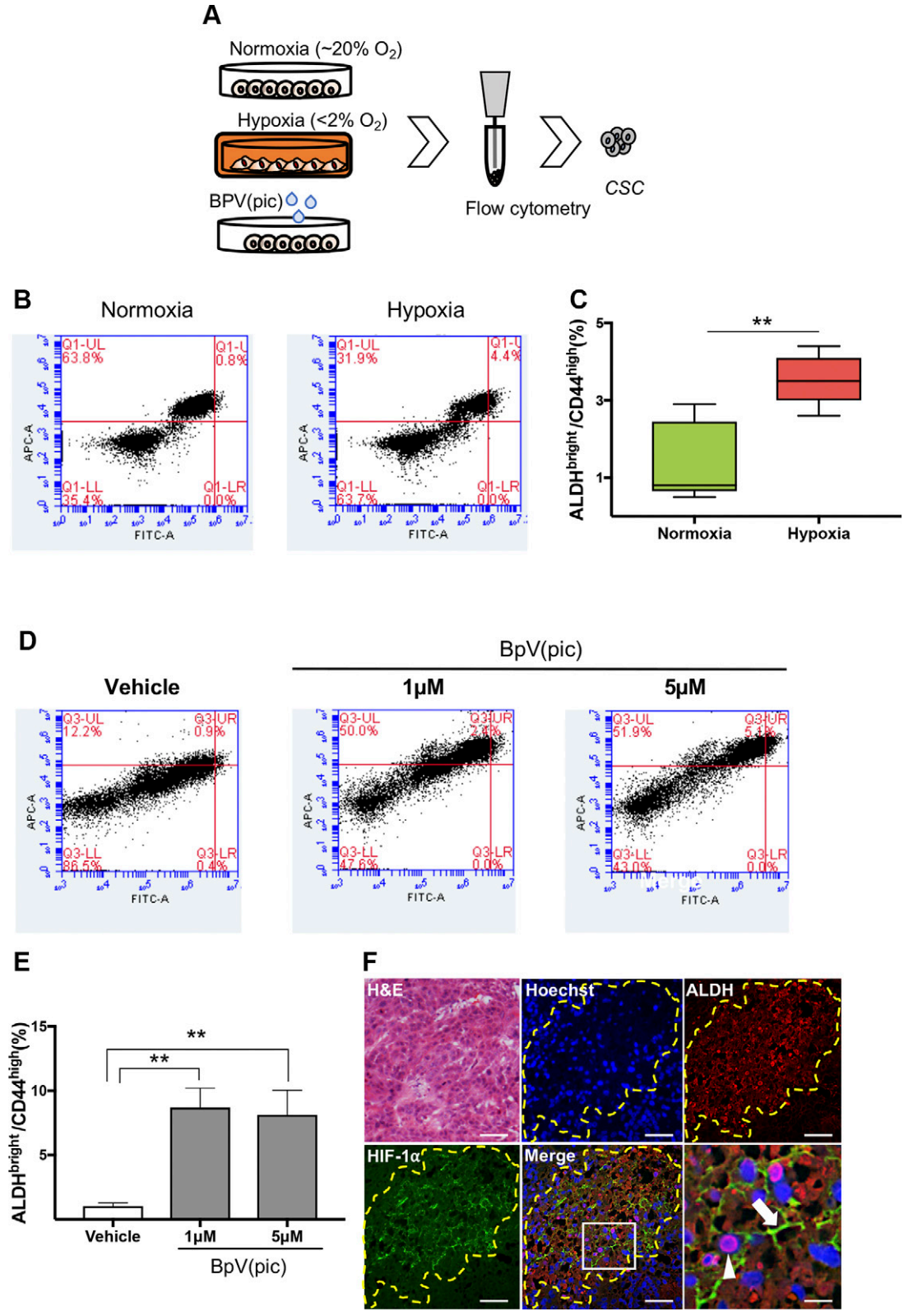

Figure 6. Accumulation of CSCs upon PTEN loss of function. *A*) Schematic representation of flow cytometry assay using HNSCC cell lines cultured under normoxia and hypoxic conditions and receiving BpV(pic). *B, C*) Tumor cells cultured under normoxia and hypoxia (12 h), showing increased levels of $ALDH^{Bright}$ and $CD44^{high}$ positive cells. Data represent means ± SEM. $*P < 0.05$. *D*) Representative graphic depicting augmented $ALDH^{Bright}$- and $CD44^{high}$-positive tumor cells receiving BpV(pic) treatment and vehicle control for 24 h. *E*) Note a concentration-dependent accumulation of $ALDH^{Bright}$ and $CD44^{high}$ positive cells upon receiving BpV(pic) for 24 h. $**P < 0.01$. *F*) Tumor-derived from HNSCC xenografts demonstrates hypoxic niches within tumor mass expressing high levels of ALDH1A1 and HIF-1α. Arrows indicate cytoplasmic expression of HIF-1α and the arrowhead indicates ALDH1A1 positive tumor cells. Scale bars, 100 μm.

triggers the accumulation of HIF-1α, and enrichment of CSCs; however, we did not know if the accumulation of CSCs is a result of the deregulation of PTEN or the expression of *HIF1A*. To better explore this signaling event, we interfered with the expression of *HIF1A* using siRNA in tumor cells growing under hypoxic conditions. We observed that loss of *HIF1A* does not interfere with the accumulation of CSCs above the observed number of positive cells growing under hypoxic conditions, suggesting that down-regulation of PTEN during hypoxic events is the leading cause of CSC accumulation (Supplemental Fig. S3*A*–*C*). Pharmacological inhibitions of PTEN resulted in similar data with the accumulation of CSCs independent from *HIF1A* expression (Supplemental Fig. S4*A*–*C*).

Increased enzymatic levels of ALDH and the presence of membrane CD44 has been validated to identify a subpopulation of cancer cells that retain high tumorigenic potential and increased self-renewal properties in HNSCC (27, 35). To further validate our findings, we used a xenograft model for HNSCC presenting hypoxic niches (Fig. 6*F*, HIF-1α). ALDH1 has 3 main isotypes, ALDH1A1, ALDH1A2, and ALDH1A3, and is a marker of normal tissue stem cells and CSCs. In order to identify CSCs within paraffin-embedded tissues, we used the ALDH1 isotype ALDH1A1, a known isotype that reflects the ALDH1 activity [reviewed in (36)]. We observed that hypoxic niches determined by high expression levels of HIF-1α are enriched with tumor cells expressing high levels of the stem cell marker ALDH1A1 (Fig. 6*F*, ALDH_Merge).

Altogether, our results suggest that the formation of hypoxic niches corroborate to the development of a unique population of neoplastic cells endowed with an aggressive phenotype and potentially refractory to therapy due to its quiescence status and the acquisition of stemness properties (**Fig. 7**).

DISCUSSION

CSCs have recently gained significant attention from the research community. Much of the interest on CSCs derives from its involvement in aggressive tumor behavior, resistance to chemotherapy, and enhanced ability to adapt to changes in the tumor microenvironment. A better understanding of the molecular circuitry that rules CSC behavior is key to the development of new therapeutic strategies to manage cancer. It is important, however, to recognize that CSCs are endowed with significant heterogeneity among tumors of different grades or between a primary and a metastatic tumor from the same patient (37, 38). Among several conditions capable of changing the behavior and number of CSCs, the accumulation of new mutations, the activation of epigenetic modifications, and changes in the tumor environmental result in forced clonal selection and variations on cancer behavior. From an environmental perspective, reduced oxygenation of tumor cells due to tumor expansion and reduced vascularization result in the development of hypoxic niches. Hypoxia impacts the tumor microenvironment in different ways that include changes in the tissue pH, resulting in poor drug performance. Interestingly, hypoxic conditions have recently been pointed out as microenvironmental cues capable of contributing to the CSC phenotype and heterogeneity (5). Although the use of antiangiogenic therapies in HNSCC is not a common practice, the formation of hypoxic areas is often seen in fast-growing head and neck tumors as demonstrated by high levels of HIF-1α$^+$ tumor cells. Most surprisingly, using colocalization assays, we show that ALDH1A1$^+$ cells (CSCs) thrive within such hypoxic niches. Indeed, low levels of hypoxia have been associated with good prognosis of HNSCC tumors (39). In search for the mechanism involved in the hypoxia-induced accumulation of CSCs, we found that the tumor suppressor *PTEN* is down-regulated in tumor cells undergoing hypoxia. Along *PTEN* down-regulation, we observed the up-regulation of the PI3K/mTOR signaling pathway during hypoxia. We further show that reduced levels of *PTEN* mediated by genetic silencing and through pharmacological inhibitions of PTEN trigger the

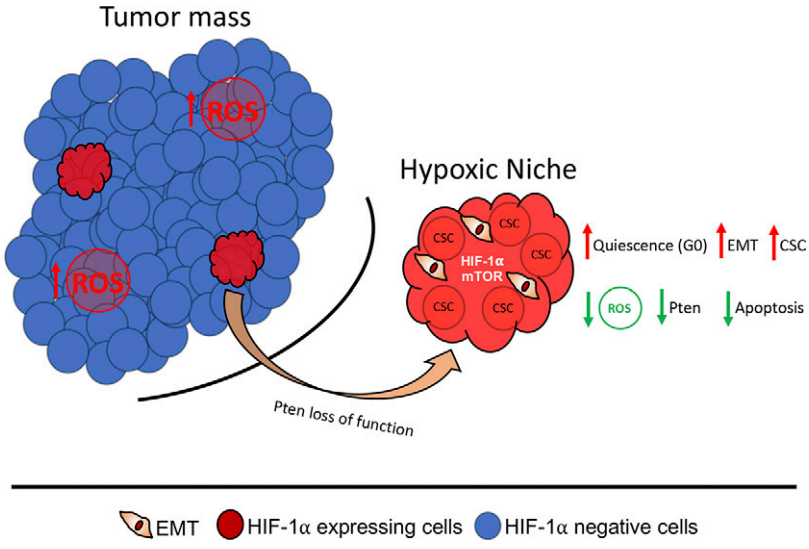

Figure 7. Schematic representation of our main findings indicates the presence of hypoxic niches in HNSCC tumors characterized by a reduced expression of PTEN. Low levels of PTEN leads to the accumulation of CSCs, along with the enhanced levels of tumor cells undergoing EMT. Along with increased invasive behavior, hypoxic niches are characterized by reduced levels of apoptosis resulted from diminished levels of ROS.

accumulation of HIF-1α$^+$ in tumor cells. Similar to our findings, the activation of mTOR is known to induce the accumulation of HIF-1α as previously reported (40, 41). Increased levels of HIF-1α has been associated with poor prognosis of colon cancer (42), pancreas (43), breast (44), peripheral nerve sheath tumors (45), lung cancer (46, 47), and HNSCC (48, 49), among others. Although high levels of mTOR are commonly reported in HNSCC and well associated to the activation of HIF-1α, the status of the tumor suppressor gene *PTEN* (master regulator of the PI3K/mTOR pathway) is far less explored in HNSCC biology. *PTEN* is found mutated in between 4 and 23% of all HNSCC, whereas the loss of protein levels is observed in >31.2% of the cases [(50), reviewed in 51]. The discrepancy between the levels of *PTEN* mutation and loss of protein expression suggests the presence of post-translational regulation mechanisms. Indeed, we have shown that accumulation of ROS in HNSCC results in PTEN oxidation and consequent loss of function (9). Here we found that protein levels of PTEN are also controlled by hypoxia. Hypoxic conditions drive down the protein levels of PTEN, and pharmacological interference of PTEN (tyrosine phosphatase inhibitors) along with gene silencing strategies result in the accumulation of HIF-1α. Therefore, we show here that compromised PTEN function results in the activation of the mTOR pathway and further accumulation of HIF-1α. Along with the accumulation of CSCs, the presence of hypoxia is also associated with the induction of EMT-like phenotype in solid tumors including hepatocellular carcinomas (52), colorectal cancer (53), hepatoblastoma, pancreatic carcinoma, breast and colon carcinomas [(54), reviewed in 55]. Here we demonstrate that the molecular mechanism of hypoxia and EMT involves the dysfunction of PTEN. Pharmacological inhibition of PTEN and NDRG2, a PTEN-binding protein responsible for the recruitment of PP2A and consequently dephosphorylation of PTEN (active form), leads to the acquisition of an EMT-like phenotype of HNSCC cells.

Overall, our findings suggest that the tumor suppressor *PTEN* acts as a guardian of CSCs and prevents the EMT-like phenotype of HNSCC. Our findings also suggest that hypoxic niches play an important role in modifying the behavior of HNSCC tumors and their CSCs. Fj

ACKNOWLEDGMENTS

This work was conducted during a visiting scholar period at the University of Michigan, sponsored by the Capes Foundation within the Brazilian Ministry of Education (Grant BEX/88881.135014/2016-01 PDSE). This work was partially supported by University of Michigan Cancer Center Support Grant P30 CA046592, and by the U.S. National Institutes of Health (NIH), National Institute of General Medical Sciences Research Grant 5R01GM120056. This grant was funded by the University of Michigan School of Dentistry faculty, and by The Robert Wood Johnson Foundation (AMFDP-72425). The monoclonal antibody AMF-17b, developed by A. B. Fulton, was obtained from the Developmental Studies Hybridoma Bank, created by the NIH Eunice Kennedy Shriver National Institute of Child Health and Human Development (NICHD) and maintained at The University of Iowa (Iowa City, IA, USA). The authors declare no conflict of interest.

AUTHOR CONTRIBUTIONS

C. H. Squarize and R. M. Castilho conceptualized the project; C. H. Squarize and R. M. Castilho designed the methodology; C. H. V. Nascimento-Filho, L. P. Webber, G. B. Borgato, C. H. Squarize, and R. M. Castilho conducted the investigation; C. H. V. Nascimento-Filho, C. H. Squarize, and R. M. Castilho wrote the original draft; C. H. V. Nascimento-Filho, E. M. Goloni-Bertollo, C. H. Squarize, and R. M. Castilho reviewed and edited the writing; C. H. Squarize and R. M. Castilho acquired funding; C. H. Squarize and R. M. Castilho located resources; and C. H. Squarize and R. M. Castilho supervised the study.

REFERENCES

1. Jemal, A., Bray, F., Center, M. M., Ferlay, J., Ward, E., and Forman, D. (2011) Global cancer statistics. *CA Cancer J. Clin.* **61**, 69–90
2. Bergers, G., and Hanahan, D. (2008) Modes of resistance to anti-angiogenic therapy. *Nat. Rev. Cancer* **8**, 592–603
3. Ebos, J. M., Lee, C. R., Cruz-Munoz, W., Bjarnason, G. A., Christensen, J. G., and Kerbel, R. S. (2009) Accelerated metastasis after short-term treatment with a potent inhibitor of tumor angiogenesis. *Cancer Cell* **15**, 232–239
4. Pàez-Ribes, M., Allen, E., Hudock, J., Takeda, T., Okuyama, H., Viñals, F., Inoue, M., Bergers, G., Hanahan, D., and Casanovas, O. (2009) Antiangiogenic therapy elicits malignant progression of tumors to increased local invasion and distant metastasis. *Cancer Cell* **15**, 220–231
5. Conley, S. J., Gheordunescu, E., Kakarala, P., Newman, B., Korkaya, H., Heath, A. N., Clouthier, S. G., and Wicha, M. S. (2012) Antiangiogenic agents increase breast cancer stem cells via the generation of tumor hypoxia. *Proc. Natl. Acad. Sci. USA* **109**, 2784–2789
6. Land, S. C., and Tee, A. R. (2007) Hypoxia-inducible factor 1alpha is regulated by the mammalian target of rapamycin (mTOR) via an mTOR signaling motif. *J. Biol. Chem.* **282**, 20534–20543
7. Hudson, C. C., Liu, M., Chiang, G. G., Otterness, D. M., Loomis, D. C., Kaper, F., Giaccia, A. J., and Abraham, R. T. (2002) Regulation of hypoxia-inducible factor 1alpha expression and function by the mammalian target of rapamycin. *Mol. Cell. Biol.* **22**, 7004–7014
8. Zagni, C., Almeida, L. O., Balan, T., Martins, M. T., Rosselli-Murai, L. K., Papagerakis, P., Castilho, R. M., and Squarize, C. H. (2017) PTEN mediates activation of core clock protein BMAL1 and accumulation of epidermal stem cells. *Stem Cell Reports* **9**, 304–314
9. Matsumoto, C. S., Almeida, L. O., Guimarães, D. M., Martins, M. D., Papagerakis, P., Papagerakis, S., Leopoldino, A. M., Castilho, R. M., and Squarize, C. H. (2016) PI3K-PTEN dysregulation leads to mTOR-driven upregulation of the core clock gene BMAL1 in normal and malignant epithelial cells. *Oncotarget* **7**, 42393–42407
10. Squarize, C. H., Castilho, R. M., Abrahao, A. C., Molinolo, A., Lingen, M. W., and Gutkind, J. S. (2013) PTEN deficiency contributes to the development and progression of head and neck cancer. *Neoplasia* **15**, 461–471
11. Zhou, J., Wulfkuhle, J., Zhang, H., Gu, P., Yang, Y., Deng, J., Margolick, J. B., Liotta, L. A., Petricoin III, E., and Zhang, Y. (2007) Activation of the PTEN/mTOR/STAT3 pathway in breast cancer stem-like cells is required for viability and maintenance. *Proc. Natl. Acad. Sci. USA* **104**, 16158–16163; erratum: 104, 19655

12. Wu, D., and Yotnda, P. (2011) Induction and testing of hypoxia in cell culture. *J. Vis. Exp.* **54**, 2899
13. Ito, A., Aoyama, T., Yoshizawa, M., Nagai, M., Tajino, J., Yamaguchi, S., Iijima, H., Zhang, X., and Kuroki, H. (2015) The effects of short-term hypoxia on human mesenchymal stem cell proliferation, viability and p16(INK4A) mRNA expression: Investigation using a simple hypoxic culture system with a deoxidizing agent. *J. Stem Cells Regen. Med.* **11**, 25–31
14. Brennan, M. D., Rexius-Hall, M. L., and Eddington, D. T. (2015) A 3D-printed oxygen control insert for a 24-well plate. *PLoS One* **10**, e0137631
15. Itoi, F., Tokoro, M., Terashita, Y., Yamagata, K., Fukunaga, N., Asada, Y., and Wakayama, T. (2012) Offspring from mouse embryos developed using a simple incubator-free culture system with a deoxidizing agent. *PLoS One* **7**, e47512
16. Faustino-Rocha, A., Oliveira, P. A., Pinho-Oliveira, J., Teixeira-Guedes, C., Soares-Maia, R., da Costa, R. G., Colaço, B., Pires, M. J., Colaço, J., Ferreira, R., and Ginja, M. (2013) Estimation of rat mammary tumor volume using caliper and ultrasonography measurements. *Lab Anim. (NY)* **42**, 217–224
17. Bousquet, P. F., Braña, M. F., Conlon, D., Fitzgerald, K. M., Perron, D., Cocchiaro, C., Miller, R., Moran, M., George, J., and Qian, X. D. (1995) Preclinical evaluation of LU 79553: a novel bis-naphthalimide with potent antitumor activity. *Cancer Res.* **55**, 1176–1180
18. Enomoto, K., Zhu, X., Park, S., Zhao, L., Zhu, Y. J., Willingham, M. C., Qi, J., Copland, J. A., Meltzer, P., and Cheng, S. Y. (2017) Targeting MYC as a therapeutic intervention for anaplastic thyroid cancer. *J. Clin. Endocrinol. Metab.* **102**, 2268–2280
19. Webber, L. P., Yujra, V. Q., Vargas, P. A., Martins, M. D., Squarize, C. H., and Castilho, R. M. (2019) Interference with the bromodomain epigenome readers drives p21 expression and tumor senescence. *Cancer Lett.* **461**, 10–20
20. Kessler, J., Hahnel, A., Wichmann, H., Rot, S., Kappler, M., Bache, M., and Vordermark, D. (2010) HIF-1α inhibition by siRNA or chetomin in human malignant glioma cells: effects on hypoxic radioresistance and monitoring via CA9 expression. *BMC Cancer* **10**, 605
21. Charafe-Jauffret, E., Monville, F., Ginestier, C., Dontu, G., Birnbaum, D., and Wicha, M. S. (2008) Cancer stem cells in breast: current opinion and future challenges. *Pathobiology* **75**, 75–84
22. Ginestier, C., Hur, M. H., Charafe-Jauffret, E., Monville, F., Dutcher, J., Brown, M., Jacquemier, J., Viens, P., Kleer, C. G., Liu, S., Schott, A., Hayes, D., Birnbaum, D., Wicha, M. S., and Dontu, G. (2007) ALDH1 is a marker of normal and malignant human mammary stem cells and a predictor of poor clinical outcome. *Cell Stem Cell* **1**, 555–567
23. Mullendore, M. E., Koorstra, J. B., Li, Y. M., Offerhaus, G. J., Fan, X., Henderson, C. M., Matsui, W., Eberhart, C. G., Maitra, A., and Feldmann, G. (2009) Ligand-dependent Notch signaling is involved in tumor initiation and tumor maintenance in pancreatic cancer. *Clin. Cancer Res.* **15**, 2291–2301
24. Dalerba, P., Dylla, S. J., Park, I. K., Liu, R., Wang, X., Cho, R. W., Hoey, T., Gurney, A., Huang, E. H., Simeone, D. M., Shelton, A. A., Parmiani, G., Castelli, C., and Clarke, M. F. (2007) Phenotypic characterization of human colorectal cancer stem cells. *Proc. Natl. Acad. Sci. USA* **104**, 10158–10163
25. Jiang, F., Qiu, Q., Khanna, A., Todd, N. W., Deepak, J., Xing, L., Wang, H., Liu, Z., Su, Y., Stass, S. A., and Katz, R. L. (2009) Aldehyde dehydrogenase 1 is a tumor stem cell-associated marker in lung cancer. *Mol. Cancer Res.* **7**, 330–338
26. Ma, S., Chan, K. W., Lee, T. K., Tang, K. H., Wo, J. Y., Zheng, B. J., and Guan, X. Y. (2008) Aldehyde dehydrogenase discriminates the CD133 liver cancer stem cell populations. *Mol. Cancer Res.* **6**, 1146–1153
27. Prince, M. E., Sivanandan, R., Kaczorowski, A., Wolf, G. T., Kaplan, M. J., Dalerba, P., Weissman, I. L., Clarke, M. F., and Ailles, L. E. (2007) Identification of a subpopulation of cells with cancer stem cell properties in head and neck squamous cell carcinoma. *Proc. Natl. Acad. Sci. USA* **104**, 973–978
28. Flores, I. L., Kawahara, R., Miguel, M. C., Granato, D. C., Domingues, R. R., Macedo, C. C., Carnielli, C. M., Yokoo, S., Rodrigues, P. C., Monteiro, B. V., Oliveira, C. E., Salmon, C. R., Nociti, F. H., Jr., Lopes, M. A., Santos-Silva, A., Winck, F. V., Coletta, R. D., and Paes Leme, A. F. (2016) EEF1D modulates proliferation and epithelial-mesenchymal transition in oral squamous cell carcinoma. *Clin. Sci. (Lond.)* **130**, 785–799
29. Nakahata, S., Ichikawa, T., Maneesaay, P., Saito, Y., Nagai, K., Tamura, T., Manachai, N., Yamakawa, N., Hamasaki, M., Kitabayashi, I., Arai, Y., Kanai, Y., Taki, T., Abe, T., Kiyonari, H., Shimoda, K., Ohshima, K., Horii, A., Shima, H., Taniwaki, M., Yamaguchi, R., and Morishita, K. (2014) Loss of NDRG2 expression activates PI3K-AKT signalling via PTEN phosphorylation in ATLL and other cancers. *Nat. Commun.* **5**, 3393
30. Ichikawa, T., Nakahata, S., Fujii, M., Iha, H., and Morishita, K. (2015) Loss of NDRG2 enhanced activation of the NF-κB pathway by PTEN and NIK phosphorylation for ATL and other cancer development. *Sci. Rep.* **5**, 12841
31. Redza-Dutordoir, M., and Averill-Bates, D. A. (2016) Activation of apoptosis signalling pathways by reactive oxygen species. *Biochim. Biophys. Acta* **1863**, 2977–2992
32. Simon, H. U., Haj-Yehia, A., and Levi-Schaffer, F. (2000) Role of reactive oxygen species (ROS) in apoptosis induction. *Apoptosis* **5**, 415–418
33. Coller, H. A. (2007) What's taking so long? S-phase entry from quiescence versus proliferation. *Nat. Rev. Mol. Cell Biol.* **8**, 667–670
34. Pardee, A. B. (1989) G1 events and regulation of cell proliferation. *Science* **246**, 603–608
35. Clay, M. R., Tabor, M., Owen, J. H., Carey, T. E., Bradford, C. R., Wolf, G. T., Wicha, M. S., and Prince, M. E. (2010) Single-marker identification of head and neck squamous cell carcinoma cancer stem cells with aldehyde dehydrogenase. *Head Neck* **32**, 1195–1201
36. Tomita, H., Tanaka, K., Tanaka, T., and Hara, A. (2016) Aldehyde dehydrogenase 1A1 in stem cells and cancer. *Oncotarget* **7**, 11018–11032
37. Anderson, K., Lutz, C., van Delft, F. W., Bateman, C. M., Guo, Y., Colman, S. M., Kempski, H., Moorman, A. V., Titley, I., Swansbury, J., Kearney, L., Enver, T., and Greaves, M. (2011) Genetic variegation of clonal architecture and propagating cells in leukaemia. *Nature* **469**, 356–361
38. Zhang, Y., Young, E. D., Bill, K., Belousov, R., Peng, T., Lazar, A. J., Pollock, R. E., Simmons, P. J., Lev, D., and Kolonin, M. G. (2013) Heterogeneity and immunophenotypic plasticity of malignant cells in human liposarcomas. *Stem Cell Res. (Amst.)* **11**, 772–781
39. Linge, A., Lock, S., Gudziol, V., Nowak, A., Lohaus, F., von Neubeck, C., Jutz, M., Abdollahi, A., Debus, J., Tinhofer, I., Budach, V., Sak, A., Stuschke, M., Balermpas, P., Rodel, C., Avlar, M., Grosu, A. L., Bayer, C., Belka, C., Pigorsch, S., Combs, S. E., Welz, S., Zips, D., Buchholz, F., Aust, D. E., Baretton, G. B., Thames, H. D., Dubrovska, A., Alsner, J., Overgaard, J., Baumann, M., and Krause, M.; DKTK-ROG (2016) Low cancer stem cell marker expression and low hypoxia identify good prognosis subgroups in HPV(-) HNSCC after postoperative radiochemotherapy: a multicenter study of the DKTK-ROG. *Clin. Cancer Res.* **22**, 2639–2649
40. Beasley, N. J., Leek, R., Alam, M., Turley, H., Cox, G. J., Gatter, K., Millard, P., Fuggle, S., and Harris, A. L. (2002) Hypoxia-inducible factors HIF-1alpha and HIF-2alpha in head and neck cancer: relationship to tumor biology and treatment outcome in surgically resected patients. *Cancer Res.* **62**, 2493–2497
41. Laughner, E., Taghavi, P., Chiles, K., Mahon, P. C., and Semenza, G. L. (2001) HER2 (neu) signaling increases the rate of hypoxia-inducible factor 1alpha (HIF-1alpha) synthesis: novel mechanism for HIF-1-mediated vascular endothelial growth factor expression. *Mol. Cell. Biol.* **21**, 3995–4004
42. Baba, Y., Nosho, K., Shima, K., Irahara, N., Chan, A. T., Meyerhardt, J. A., Chung, D. C., Giovannucci, E. L., Fuchs, C. S., and Ogino, S. (2010) HIF1A overexpression is associated with poor prognosis in a cohort of 731 colorectal cancers. *Am. J. Pathol.* **176**, 2292–2301
43. Miyake, K., Yoshizumi, T., Imura, S., Sugimoto, K., Batmunkh, E., Kanemura, H., Morine, Y., and Shimada, M. (2008) Expression of hypoxia-inducible factor-1alpha, histone deacetylase 1, and metastasis-associated protein 1 in pancreatic carcinoma: correlation with poor prognosis with possible regulation. *Pancreas* **36**, e1–e9
44. Gruber, G., Greiner, R. H., Hlushchuk, R., Aebersold, D. M., Altermatt, H. J., Berclaz, G., and Djonov, V. (2004) Hypoxia-inducible factor 1 alpha in high-risk breast cancer: an independent prognostic parameter? *Breast Cancer Res.* **6**, R191–R198
45. Fukushima, S., Endo, M., Matsumoto, Y., Fukushi, J. I., Matsunobu, T., Kawaguchi, K. I., Setsu, N., IIda, K., Yokoyama,

N., Nakagawa, M., Yahiro, K., Oda, Y., Iwamoto, Y., and Nakashima, Y. (2017) Hypoxia-inducible factor 1 alpha is a poor prognostic factor and potential therapeutic target in malignant peripheral nerve sheath tumor. *PLoS One* **12**, e0178064; erratum: 13, e0194508
46. Lin, C. S., Liu, T. C., Lee, M. T., Yang, S. F., and Tsao, T. C. (2017) Independent prognostic value of hypoxia-inducible factor 1-alpha expression in small cell lung cancer. *Int. J. Med. Sci.* **14**, 785–790
47. Hung, J. J., Yang, M. H., Hsu, H. S., Hsu, W. H., Liu, J. S., and Wu, K. J. (2009) Prognostic significance of hypoxia-inducible factor-1alpha, TWIST1 and Snail expression in resectable non-small cell lung cancer. *Thorax* **64**, 1082–1089
48. Aebersold, D. M., Burri, P., Beer, K. T., Laissue, J., Djonov, V., Greiner, R. H., and Semenza, G. L. (2001) Expression of hypoxia-inducible factor-1alpha: a novel predictive and prognostic parameter in the radiotherapy of oropharyngeal cancer. *Cancer Res.* **61**, 2911–2916
49. Roh, J. L., Cho, K. J., Kwon, G. Y., Ryu, C. H., Chang, H. W., Choi, S. H., Nam, S. Y., and Kim, S. Y. (2009) The prognostic value of hypoxia markers in T2-staged oral tongue cancer. *Oral Oncol.* **45**, 63–68
50. Feldman, R., Gatalica, Z., Knezetic, J., Reddy, S., Nathan, C. A., Javadi, N., and Teknos, T. (2016) Molecular profiling of head and neck squamous cell carcinoma. *Head Neck* **38**(Suppl 1), E1625–E1638
51. Giudice, F. S., and Squarize, C. H. (2013) The determinants of head and neck cancer: Unmasking the PI3K pathway mutations. *J. Carcinog. Mutagen.* (Suppl 5), **2013**, 003
52. Zhang, L., Huang, G., Li, X., Zhang, Y., Jiang, Y., Shen, J., Liu, J., Wang, Q., Zhu, J., Feng, X., Dong, J., and Qian, C. (2013) Hypoxia induces epithelial-mesenchymal transition via activation of SNAI1 by hypoxia-inducible factor -1α in hepatocellular carcinoma. *BMC Cancer* **13**, 108
53. Choi, B. J., Park, S. A., Lee, S. Y., Cha, Y. N., and Surh, Y. J. (2017) Hypoxia induces epithelial-mesenchymal transition in colorectal cancer cells through ubiquitin-specific protease 47-mediated stabilization of Snail: a potential role of Sox9. *Sci. Rep.* **7**, 15918
54. Cannito, S., Novo, E., Compagnone, A., Valfrè di Bonzo, L., Busletta, C., Zamara, E., Paternostro, C., Povero, D., Bandino, A., Bozzo, F., Cravanzola, C., Bravoco, V., Colombatto, S., and Parola, M. (2008) Redox mechanisms switch on hypoxia-dependent epithelial-mesenchymal transition in cancer cells. *Carcinogenesis* **29**, 2267–2278
55. Cannito, S., Novo, E., di Bonzo, L. V., Busletta, C., Colombatto, S., and Parola, M. (2010) Epithelial-mesenchymal transition: from molecular mechanisms, redox regulation to implications in human health and disease. *Antioxid. Redox Signal.* **12**, 1383–1430

Received for publication March 22, 2019.
Accepted for publication August 26, 2019.